Progress In Electromagnetics Research, PIER 67, 181–203, 2007

MICROWAVE EMISSION FROM TWO-DIMENSIONAL INHOMOGENEOUS DIELECTRIC ROUGH SURFACES BASED ON PHYSICS-BASED TWO-GRID METHOD

K. S. Chen

Center for Space and Remote Sensing Research
National Central University
Chung-Li, Taiwan 32054

L. Tsang

Department of Electrical Engineering, Box 352500
University of Washington
Seattle, WA 98195, USA

J. C. Shi

Institute for Computational Earth System Science
University of California
Santa Barbara, CA 93106, USA

H. C. Huang

INTEL
Hillsboro, OR 97124, USA

Abstract—Numerical simulations of emission for two-dimensional randomly rough surfaces with an inhomogeneous layered medium are presented. The inhomogeneous layered medium is modeled by a generalized n-layered stratified media. The numerical method was adopted from the physics-based two-grid method (PBTG). To ensure the strict accuracy requirement while to relief the memory and CPU resources, the PBTG in conjunction with the sparse-matrix canonical grid method (SMCG) was used in this paper. In so doing the reflected terms of the dyadic Green's function that accounts for layered media were added into the integral equations governing the surface tangential fields. Since the reflected part of the dyadic Green's function does not

contain any singularity, the normal components of the fields remain the same as in the case of homogeneous surfaces. It was found that the elements of Green's tensor are only important to the near-field since they decay very fast as spatial distance goes beyond a few wavelengths. The resulting integral equations are then solved by the Method of Moment (MoM). Comparisons between the inhomogeneous and the homogeneous rough surfaces suggest that the presence of the inhomogeneous layered medium has non-negligible contributions to emission, depending on the dielectric gradient and is polarization dependent.

1. INTRODUCTION

Natural surfaces such as soil, snow-covered, and frozen ground surfaces are better modeled as inhomogeneous dielectric rough surface where variations exist both in surface height and subsurface permittivity. Understanding of electromagnetic wave scattering and emission from a two-dimensional inhomogeneous dielectric rough surface are of interest to both remote sensing (soil moisture, sea ice, frozen land, etc.) and optical imaging [1–12]. Among the various numerical methods, Pelosi and Coccioli [13] applied a finite element method based on perturbation formulation to deal with one-dimensional slightly rough surfaces with multiple scattering being neglected. In [14], both differential method and integral method were adopted to study the scattering from randomly rough inhomogeneous films. They are able to treat the surface and volume scattering by means of boundary-integral method. Again, the surface considered was in one-dimensional.

From practical applications point of view, it is desirable to have a numerical simulation of two-dimensional rough surfaces. where the roughness heights vary in both horizontal directions. The most common method that has been used in numerical simulations is the surface integral equation method and its solution by the method of moments (MoM) [15–17]. It has been shown that the physics-based two-grid method (PBTG) can efficiently compute the accurate surface fields on the dense grid in terms of CPU time and memory requirements [18, 19]. Thus the PBTG in conjunction with the sparse-matrix canonical grid method (SMCG) is adopted in this paper.

With the fast and yet accurate numerical simulation method at hands, it is not difficult to study the effects of the surface inhomogeneity on the microwave emissions. By viewing the Green's function of layered inhomogeneous media, it is noted that the reflect term that accounts for the inhomogeneous effects is needed in addition

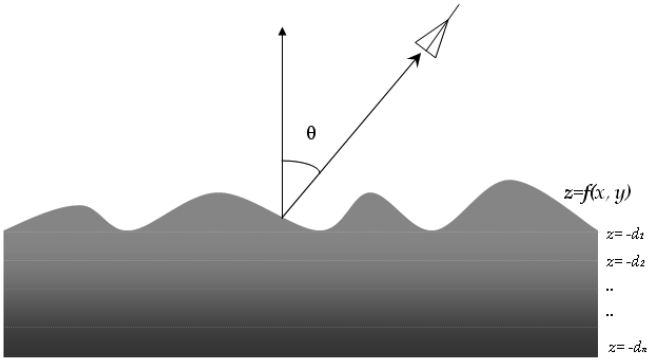

Figure 1. Geometry of a rough surface with a layered medium $\varepsilon(\vec{r})$ modeled by N layers of piecewise constant regions.

to a direct term. The original PBTG along with SCM is unchanged for the direct term. What is needed is to add on the reflect term. Mathematically, this is simple and straightforward. Numerically, it is not really so, however. After some mathematical manipulations, it is possible to split the reflect term, and cast them into the original algorithm with minimum modifications. Comparisons between the inhomogeneous and homogeneous rough surfaces suggest that the presence of the inhomogeneous layered medium has non-negligible contributions depending on the frequency and observation angle. In the following section, the formulations that govern the wave interactions with the inhomogeneous rough surfaces are given. Numerical solution by the PBTG method is described. Numerical simulation results are then discussed. Finally, a summary is drawn.

2. FORMULATION OF THE PROBLEM

Consider a plane wave, $\vec{E}_i(\vec{r})$ and $\vec{H}_i(\vec{r})$, with a time dependence of $e^{-i\omega t}$, impinging upon a two-dimensional dielectric rough surface [Fig. 1] with a random height of $z = f(x, y)$. The incident fields can be expressed in terms of spectrum of the incident wave [15]

$$\vec{E}_i(\vec{r}) = \int_{-\infty}^{+\infty} dk_x \int_{-\infty}^{+\infty} dk_y \exp(ik_x x + ik_y y - ik_z z)\tilde{E}(k_x, k_y)\hat{e}(-k_z) \quad (1)$$

$$\vec{H}_i(\vec{r}) = -\frac{1}{\eta} \int_{-\infty}^{+\infty} dk_x \int_{-\infty}^{+\infty} dk_y \exp(ik_x x + ik_y y - ik_z z)\tilde{E}(k_x, k_y)\hat{h}(-k_z) \quad (2)$$

For TE wave incidence

$$\hat{e}(-k_z) = \frac{1}{k_\rho}(\hat{x}k_y - \hat{y}k_x) \tag{3}$$

$$\hat{h}(-k_z) = \frac{k_z}{kk_\rho}(\hat{x}k_x - \hat{y}k_y) + \frac{k_\rho}{k}\hat{z} \tag{4}$$

and for TM wave incidence

$$\hat{h}(-k_z) = -\frac{1}{k_\rho}(\hat{x}k_y - \hat{y}k_x) \tag{5}$$

$$\hat{e}(-k_z) = \frac{k_z}{kk_\rho}(\hat{x}k_x + \hat{y}k_y) + \frac{k_\rho}{k}\hat{z} \tag{6}$$

with $k_z = \sqrt{k^2 - k_\rho^2}$ and $k_\rho = \sqrt{k_x^2 + k_y^2}$. The incident wave vector is $\hat{k}_i = \sin\theta_i\cos\phi_i\hat{x} + \sin\theta_i\sin\phi_i\hat{y} - \cos\theta_i\hat{z}$, and $\hat{e}, \hat{h}$ denote the polarization vectors. In the above k and η are the wavenumber and wave impedance of free space, respectively. In practical cases, the incident field is tapered so that the illuminated rough surface can be confined to the surface area $L_x \times L_y$ [15]. The spectrum of the incident wave, $\tilde{E}(k_x, k_y)$, is given as

$$\begin{aligned}\tilde{E}(k_x, k_y) = {} & \frac{1}{4\pi^2}\int_{-\infty}^{+\infty} dx \int_{-\infty}^{+\infty} dy \exp(-ik_x x - ik_y y) \\ & \times \exp[i(k_{ix}x + k_{iy}y)(1+w)]\exp(-\Theta)\end{aligned} \tag{7}$$

where $\Theta = \Theta_x + \Theta_y = (x^2 + y^2)/g^2$ and

$$\Theta_x = \frac{(\cos\theta_i\cos\phi_i x + \cos\theta_i\sin\phi_i y)^2}{g^2\cos^2\theta_i} \tag{8}$$

$$\Theta_y = \frac{(-\sin\phi_i x + \cos\phi_i y)^2}{g^2} \tag{9}$$

$$w = \frac{1}{k_1^2}\left(\frac{2\Theta_x - 1}{g^2\cos^2\theta_i} + \frac{2\Theta_y - 1}{g^2}\right) \tag{10}$$

The parameter g controls the tapering of the incident wave.

With the incident waves defined above, now the surface fields satisfy equations [15, 18]:

$$\vec{E}_i + \int \left[i\varpi\mu_0 \overline{\overline{G}}_0 \cdot \hat{n}' \times \vec{H}(\vec{r}') + \nabla' \times \overline{\overline{G}}_0 \cdot \hat{n}' \times \vec{E}(\vec{r}') \right] dS' = \begin{cases} \vec{E}(\vec{r}), & z < f \\ 0, & z > f \end{cases} \tag{11}$$

$$\int \left[-i\varpi\mu_1 \overline{\overline{G}}_1 \cdot \hat{n}' \times \vec{H}_1(\vec{r}') - \nabla' \times \overline{\overline{G}}_1 \cdot \hat{n}' \times \vec{E}_1(\vec{r}') \right] dS' = \begin{cases} 0, & z < f \\ \vec{E}_1(\vec{r}), & z < f \end{cases} \tag{12}$$

$$\vec{H}_i + \int \left[-ik/\eta \overline{\overline{G}}_0 \cdot \hat{n}' \times \vec{E}(\vec{r}') + \nabla' \times \overline{\overline{G}}_0 \cdot \hat{n}' \times \vec{H}(\vec{r}') \right] dS' = \begin{cases} \vec{H}(\vec{r}), & z > f \\ 0, & z < f \end{cases} \tag{13}$$

$$\int \left[-ik/\eta \overline{\overline{G}}_1 \cdot \hat{n}' \times \vec{E}_1(\vec{r}') + \nabla' \times \overline{\overline{G}}_1 \cdot \hat{n}' \times \vec{H}_1(\vec{r}') \right] dS' = \begin{cases} 0, & z > f \\ \vec{H}_1(\vec{r}), & z < f \end{cases} \tag{14}$$

where S' denotes the rough surface, $\vec{r}'$ a source point and a field point on the rough surface. The unit normal vector $\hat{n}'$ refers to primed coordinate and points away from the second medium.

The dyadic Green's functions of free space, $\overline{\overline{G}}_0$, is

$$\overline{\overline{G}}_0(\vec{r}, \vec{r}') = \frac{\left[\overline{\overline{I}} + \nabla\nabla/k^2 \right] e^{ik|\vec{r} - \vec{r}'|}}{4\pi|\vec{r} - \vec{r}'|} \tag{15}$$

where $\overline{\overline{I}}$ is unit dyadic. The dyadic Green's function of the lower medium, an inhomogeneous layer, $\overline{\overline{G}}_1$, consists of two parts: a direct part and a reflected part:

$$\overline{\overline{G}}_1(\vec{r}, \vec{r}') = \overline{\overline{G}}_1^d(\vec{r}, \vec{r}') + \overline{\overline{G}}_1^r(\vec{r}, \vec{r}') \tag{16}$$

The direct part $\overline{\overline{G}}_1^d(\vec{r}, \vec{r}')$ is the same as the one for homogeneous medium

$$\overline{\overline{G}}_1^d(\vec{r}, \vec{r}') = \frac{\left[\overline{\overline{I}} + \nabla\nabla/k_1^2 \right] e^{ik_1|\vec{r} - \vec{r}'|}}{4\pi|\vec{r} - \vec{r}'|}, \tag{17}$$

which can be put into a vector form and the reflected part $\overline{\overline{G}}_1^r(\vec{r},\vec{r}\,')$ that accounts for the layered effects is given as [1, 2]

$$\begin{aligned}\overline{\overline{G}}_1^r(\vec{r},\vec{r}\,') &= \frac{-\iota}{8\pi^2}\int dk_x dk_y e^{ik_x(x-x')+ik_y(y-y')}e^{ik_{1z}(z+z')} \\ &\quad\times\left[R^{TE}\hat{e}(k_{1z})\hat{e}(-k_{1z})+R^{TM}\hat{h}(k_{1z})\hat{h}(-k_{1z})\right] \quad (18)\end{aligned}$$

where

$$\hat{e}(k_{1z}) = \hat{e}(-k_{1z}) = \frac{1}{k_\rho}(\hat{x}k_y - \hat{y}k_x) \quad (19)$$

$$\hat{h}(k_{1z}) = \frac{-k_{1z}}{k_1 k_\rho}(\hat{x}k_x + \hat{y}k_y) + \frac{k_\rho}{k_1}\hat{z} \quad (20)$$

$$\hat{h}(-k_{1z}) = \frac{k_{1z}}{k_1 k_\rho}(\hat{x}k_x + \hat{y}k_y) + \frac{k_\rho}{k_1}\hat{z} \quad (21)$$

The reflection coefficients for TE (horizontal) and TM (vertical) polarizations, R^{TE} and R^{TM}, respectively, are readily obtained through the recurrence relation [1, 2] assuming that the general inhomogeneous layer is represented by N layers of piecewise constant regions (see Fig. 1). This formulation is applicable if the first layered medium interface is below the lowest point of the rough surface $f(x, y)$, i.e., $f(x, y) \geq -d_1$. To evaluate (18), a double infinite integral is required to compute. The numerical approach proposed in [20] is applied in this paper. As a result, a total of nine elements of $\overline{\overline{G}}_1^r$ and a total of eight elements of $\nabla \times \overline{\overline{G}}_1^r$ are numerically evaluated. These elements represent the contributions from the inhomogeneous layers to the total scattering. The reformulation is given in next section, while the complete components for numerical computation are given in Appendix. When the lower medium is homogeneous, $\overline{\overline{G}}_1^r(\vec{r},\vec{r}\,')$ vanishes, and the problem reduces to those homogeneous rough surface scattering as treated in [18, 19] by the physics-based two-grid method (PBTG). In the next section, we will briefly give some background about PBTG, followed by the application of PBTG including the layered medium.

Once the surface fields are solved, the scattered fields at far zone can be computed according to the Stratton and Chu formula

$$\vec{E}^s = \frac{ike^{ikR}}{4\pi R}\left(\overline{\overline{I}} - \hat{k}_s\hat{k}_s\right)\int\left\{\hat{k}_s \times [\hat{n}\times\vec{E} + \eta\hat{n}\times\vec{H}]\right\}e^{-ik_s\hat{k}_s\cdot\vec{r}\,'}dS' \quad (22)$$

The scattering vector is $\hat{k}_s = \sin\theta_s\cos\phi_s\hat{x} + \sin\theta_s\sin\phi_s\hat{y} + \cos\theta_s\hat{z}$. The α polarized scattered field is $E^s_\alpha = \hat{\alpha}\cdot\vec{E}^s$.

For an incident wave with a polarization b, the scattering coefficient is

$$\sigma_{\alpha\beta}(\theta_s, \phi_s; \theta_i, \varphi_i) = \frac{|E_\alpha^s|^2}{2\eta_1 P_\beta^{inc}} \tag{23}$$

where the incident power is

$$P_\beta^{inc} = \frac{2\pi^2}{\eta} \int\limits_{k_\rho < k} dk_x dk_y \left|\tilde{E}(k_x, k_y)\right|^2 \frac{k_z}{k} \tag{24}$$

For scattering by a dielectric surface, the reflectivity and emissivity of the rough surface at incident angle (θ_i, ϕ_i) (observation angle in emission because of reciprocity) are, respectively,

$$\Gamma_\alpha(\theta_i, \phi_i) = \frac{1}{4\pi} \iint [\sigma_{\alpha\alpha}(\theta_s, \phi_s; \theta_i, \varphi_i) + \sigma_{\alpha\beta}(\theta_s, \phi_s; \theta_i, \varphi_i)] \sin\theta_s d\theta_s d\phi \tag{25}$$

$$e_\alpha(\theta_i, \phi_i) = 1 - \Gamma\alpha(\theta_i, \phi_i) \tag{26}$$

Because of reciprocity, emissivity is the same as absorptivity, the amount of power absorbed by the dielectric in a scattering problem. In passive remote sensing, the brightness temperature T_B of the medium is measured at observation angle (θ_i, ϕ_i). The brightness temperature is

$$T_B(\theta_i, \phi_i) = e_\alpha(\theta_i, \phi_i) T_p \tag{27}$$

(27) where T_p is physical temperature of the medium in degrees Kelvin. It is important that the scattering calculation obey energy conservation to less than 1% [18], so that the error in brightness temperature is limited to less than 3 K for room temperature.

3. A PBTG-BASED SOLUTION OF INTEGRAL EQUATIONS FOR A ROUGH SURFACE WITH LAYERED MEDIUM

3.1. The Physics-Based Two-Grid Method

In this section, we briefly give an introduction of PBTG method for the case of homogeneous surfaces. In the next section, we then show that how the reflected part of the dyadic Green's function is cast into formulation such that the modification of the numerical coding can be minimized within the framework of the PBTG. In the development of PBTG for the homogeneous rough surfaces [18], equations (1)–(4) are

written in the matrix equations using moment of method with pulse function as basis function and point matching method

$$\sum_{n=1}^{N}\left[Z_{mn}^{p1}I_n^{(1)}+Z_{mn}^{p2}I_n^{(2)}+Z_{mn}^{p3}I_n^{(3)}+Z_{mn}^{p4}I_n^{(4)}+Z_{mn}^{p5}I_n^{(5)}+Z_{mn}^{p6}I_n^{(6)}\right] = I_m^{(p)inc} \quad (28)$$

where $I_n^{(q)}$ are unknown surface fields needed to be solved, and $I_m^{(p)inc}$ are given by the incident fields, and the parameter N is the number of points we use to sample the rough surface. For $p = 1, 2, 3$ which correspond the surface integral equation when approaching the surface from free space and for $p = 4, 5, 6$ when approaching the surface from the lower medium. The quantities of $I_m^{(p)inc}$ are zero for $p = 4, 5, 6$.

Where

$$I_n^{(1)} = F_x(\vec{r}) = S_{xy}(\vec{r}_n)[\hat{n}\times\vec{H}(\vec{r}_n)]\cdot\hat{x} \quad (29)$$

$$I_n^{(2)} = F_y(\vec{r}) = S_{xy}(\vec{r}_n)[\hat{n}\times\vec{H}(\vec{r}_n)]\cdot\hat{y} \quad (30)$$

$$I_n^{(3)} = I_n(\vec{r}) = S_{xy}(\vec{r}_n)\hat{n}\cdot\vec{E}(\vec{r}_n) \quad (31)$$

$$I_n^{(4)} = I_x(\vec{r}) = S_{xy}(\vec{r}_n)[\hat{n}\times\vec{E}(\vec{r}_n)]\cdot\hat{x} \quad (32)$$

$$I_n^{(5)} = I_y(\vec{r}) = S_{xy}(\vec{r}_n)[\hat{n}\times\vec{E}(\vec{r}_n)]\cdot\hat{y} \quad (33)$$

$$I_n^{(6)} = F_n(\vec{r}) = S_{xy}(\vec{r}_n)\hat{n}\cdot\vec{H}(\vec{r}_n) \quad (34)$$

are surface unknowns and $S_{xy} = \sqrt{1+f_x^2+f_y^2},\ f_x = \frac{\partial f}{\partial x},\ f_y = \frac{\partial f}{\partial y}$.

The Z_{mn}^{pq} in (28) are the impedance elements and are determined by the free space Green's function and the lower medium Green's function. The parameter N is the number of points we use to digitize the rough surface.

To solve equation (28), the surface fields can be obtained. Traditionally, the matrix equation is solved by matrix inversion or Gaussian elimination methods, which require $O(N^3)$ operations and $O(N^2)$ memory. In the physics-based two-grid method, two grids with sampling points per wavelength of n_{scg} (coarse grid) and n_{sdg} (dense grid), respectively, are used. The PBTG is used in conjunction with the SMCG that was previously used in computing scattering from 2-dimensional rough surfaces. By ignoring the pre-multiplication, post-multiplication, and interpolation calculations and retaining only the dominant terms, the total number of operations (multiplications) is

approximately [15, 18]

$$\begin{aligned} & N_{CGM}\left[256r_l^2 n_{sdg} N_{sdg}\right] \\ & +N_{CGM}\left[256\left(r_d^2 - r_l^2\right) n_{scg} N_{scg} + 2N_{scg}\log(N_{scg}) m_{FFT}\right] \\ & +N_{SMCG}\left[72N_{scg}\log(N_{scg}) m_{FFT}\right] \end{aligned} \quad (35)$$

where N_{CGM} and N_{SMCG} are the number of iterations in the conjugate gradient method (CGM) matrix solver and the number of right-hand-side updates, respectively, n_{sdg} and n_{scg} are the number of sample points per λ^2 on the dense and coarse grids, respectively, and m_{FFT} is the total number of FFT's and inverse FFT's.

3.2. Inclusion of Reflected Part of the Dyadic Green's Function

To keep the structure of the PBTG algorithm as much as possible, the surface fields associated with the reflected part of the dyadic Green's function is decomposed into tangential and normal components for $\vec{E}$ and $\vec{H}$ fields. For inhomogeneous surfaces, there are additional tangential fields, $\hat{n}\times\vec{E},\ \vec{n}\times\vec{H}$ associated with the $\overline{\overline{G}}_1^r,\ \nabla\times\overline{\overline{G}}_1^r$ and normal fields, $\hat{n}\cdot\vec{E},\ \vec{n}\cdot\vec{H}$ associated with $\nabla\overline{\overline{G}}_1^r$ need to be solved. In the following, we illustrate our derivation for the reflected part of the Green's function. The final results can be put into the structure of PBTG and thus the fast method can be applied.

Consider the integral equation of the form

$$\vec{E} = \vec{E}^i + \int\left\{\nabla\times\overline{\overline{G}}_1^r\cdot(\hat{n}'\times\vec{E}) + j\omega\mu\overline{\overline{G}}_1^r\cdot(\hat{n}'\times\vec{H})\right\}dS' \quad (36)$$

$$\vec{H} = \vec{H}^i + \int\left\{-j\omega\varepsilon\overline{\overline{G}}_1^r\cdot(\hat{n}'\times\vec{E}) + \nabla\times\overline{\overline{G}}_1^r\cdot(\hat{n}'\times\vec{H})\right\}dS' \quad (37)$$

Taking the tangential projection, we reach the following form

$$\hat{n}\times\vec{E} = \hat{n}'\times\vec{E}^i + \hat{n}\times\int\left\{\nabla\times\overline{\overline{G}}_1^r\cdot(\hat{n}'\times\vec{E}) + j\omega\mu\overline{\overline{G}}_1^r\cdot(\hat{n}'\times\vec{H})\right\}dS' \quad (38)$$

$$\hat{n}\times\vec{H} = \hat{n}\times\vec{H}^i + \hat{n}\times\int\left\{-j\omega\varepsilon\overline{\overline{G}}_1^r\cdot(\hat{n}'\times\vec{E}) + \nabla\times\overline{\overline{G}}_1^r\cdot(\hat{n}'\times\vec{H})\right\}dS' \quad (39)$$

Following the notations of PBTG, (38) and (39) can be rewritten as

$$\vec{I}^r = (\vec{s}\times\vec{E}^i) + \vec{s}\times\iint\left(\nabla\times\overline{\overline{G}}_1^r\cdot\vec{I}^{r'} + j\omega\mu\overline{\overline{G}}_1^r\cdot\vec{F}^{r'}\right)dx'dy' \quad (40)$$

$$\vec{F}^r = (\vec{s} \times \vec{H}^i) + \vec{s} \times \iint \left(-j\omega\varepsilon \overline{\overline{G}}_1^r \cdot \vec{I}^{r'} + \nabla \times \overline{\overline{G}}_1^r \cdot \vec{F}^{r'} \right) dx'dy' \quad (41)$$

What we need is to write up explicit forms of $\vec{I}^r$ and $\vec{F}^r$. This is given in Appendix A. Now that the $I_x^r, I_y^r, I_n^r, F_x^r, F_y^r, F_n^r$ are new terms resulting from $\overline{\overline{G}}_1^r$ and are readily added on the original six scalar integral equations for the homogeneous medium. The rewritten $I_x^r, I_y^r, I_n^r, F_x^r, F_y^r, F_n^r$ makes the inclusion of the inhomogeneous effects without difficulties by simply casting them into the PBTG framework. The inclusions of these terms in generation of impedance matrix slightly increase the computation time. Numerically calculations involving $\overline{\overline{G}}_1^r$ and $\nabla \times \overline{\overline{G}}_1^r$ are illustrated below.

3.3. Computations of the $\overline{\overline{G}}_1^r$ and $\nabla \times \overline{\overline{G}}_1^r$

As the formulations made in the above section, the inclusion of the reflected part of the dyadic Green's function that accounts for the inhomogeneity of the lower medium under the framework PBTG method is straightforward. In forming the impedance matrix and thus in the calculation of the matrix elements, additional efforts must be exercised to compute the matrix elements with double infinite integral involving $\overline{\overline{G}}_1^r$ and $\nabla \times \overline{\overline{G}}_1^r$. In this aspect, we adopted the method proposed by Tsang et al. [20]. The method evaluates the matrix elements by numerically integrating the Sommerfeld integrals along the Sommerfeld with higher order asymptotic extraction.

Written in spectral form,

$$\begin{aligned}
\overline{\overline{G}}_1^r(\vec{r}, \vec{r}') &= \frac{i}{8\pi^2} \iint dk_x dk_y \frac{1}{k_{1z}} \Big[R^{TE} \hat{e}(k_{1z}) \hat{e}(-k_{1z}) \\
&\quad + R^{TM} \hat{h}(k_{1z}) \hat{h}(-k_{1z}) \Big] \\
&\quad \times e^{ik_x(x-x') + ik_y(y-y') + ik_{1z}(z+z')} \\
&= \frac{i}{8\pi^2} \iint dk_x dk_y \frac{1}{k_{1z}} \Big[R^{TE} e^{-2ik_{1z}d_1} \hat{e}(k_{1z}) \hat{e}(-k_{1z}) \\
&\quad + R^{TM} e^{-2ik_{1z}d_1} \hat{h}(k_{1z}) \hat{h}(-k_{1z}) \Big] \\
&\quad \times e^{ik_x(x-x') + ik_y(y-y') + ik_{1z}(z+z'+2d_1)}
\end{aligned} \quad (42)$$

The curl of (42) is

$$\begin{aligned}
\nabla \times \overline{\overline{G}}_1^r(\vec{r}, \vec{r}') &= \frac{i}{8\pi^2} \iint dk_x dk_y \frac{1}{k_{1z}} \Big[R^{TE} \hat{h}(k_{1z}) \hat{e}(-k_{1z}) \\
&\quad + R^{TM} \hat{e}(k_{1z}) \hat{h}(-k_{1z}) \Big]
\end{aligned}$$

$$\begin{aligned} &\times e^{ik_x(x-x')+ik_y(y-y')+ik_{1z}(z+z')} \\ = &\frac{i}{8\pi^2}\iint dk_x dk_y \frac{1}{k_{1z}}\left[R^{TE}e^{-2ik_{1z}d_1}\hat{h}(k_{1z})\hat{e}(-k_{1z})\right. \\ &\left.+ R^{TM}e^{-2ik_{1z}d_1}\hat{e}(k_{1z})\hat{h}(-k_{1z})\right] \\ &\times e^{ik_x(x-x')+ik_y(y-y')+ik_{1z}(z+z'+2d_1)} \end{aligned} \tag{43}$$

More explicit forms of (42) and (43) are given in Appendix B. Following the numerical procedures proposed in [20], they are calculated in high numerical stability and accuracy. Finally, the reflection coefficients R^{TM}, R^{TE} are given for completeness [1, 2].

$$\begin{aligned} R^p = &\frac{e^{i2k_z d_0}}{R^p_{01}} + \frac{\left[1-(1/R^p_{01})^2\right]e^{i2(k_{1z}+k_z)d_0}}{(1/R^p_{01})e^{i2k_{1z}d_0}} + \frac{e^{i2k_{1z}d_1}}{R^p_{12}} \\ &+\frac{\left[1-(1/R^p_{12})^2\right]e^{i2(k_{2z}+k_{1z})d_1}}{(1/R^p_{12})e^{i2k_{2z}d_1}} + \cdots + \frac{e^{i2k_{(l-1)z}d_{l-1}}}{R^p_{(l-1)l}} \\ &+\frac{\left[1-(1/R^p_{(l-1)l})^2\right]e^{i2(k_{lz}+k_{(l-1)z})d_{l-1}}}{(1/R^p_{(l-1)l})e^{i2k_{lz}d_{l-1}}} + R_{lt}e^{i2k_{lz}d_l} \end{aligned} \tag{44}$$

where $p = TE$ or TM, $l = 1, 2, \ldots, N$ and d_l represents region depth in region l.

Fig. 2 and Fig. 3 present two cases of emissivity of a three-layered medium. The top boundary was assumed to be plane. When the permittivity of the first layer is lower, the angular curve of the emissivity tends to be more flat.

4. NUMERICAL RESULTS AND DISCUSSIONS

Simulations were conducted on Gaussian rough surfaces with correlation length of 1 wavelength, *rms* height of 0.1 wavelength, and the relative dielectric constant of $7.35+i0.8725$. For the lower dielectric medium, an inhomogeneous layered medium with three layers was chosen. The depths of the layer 1 and layer 2 were, respectively, 0.25 and 1 wavelength, with relative dielectric constants of $7.35 + i0.8725$ and $8.3 + i1.0$, respectively. Half-space background was assumed with dielectric constant of $9.3 + i1.335$. The total scattering power was then simulated averaged over 5 realizations. It is noted that unlike in the active sensing, fewer realizations are required in the passive sensing simulation because of a large number of angular observations available for ensemble average. In [18], it has been shown that 5 realizations can give sufficiently accurate results. Table 1 gives the total scattering

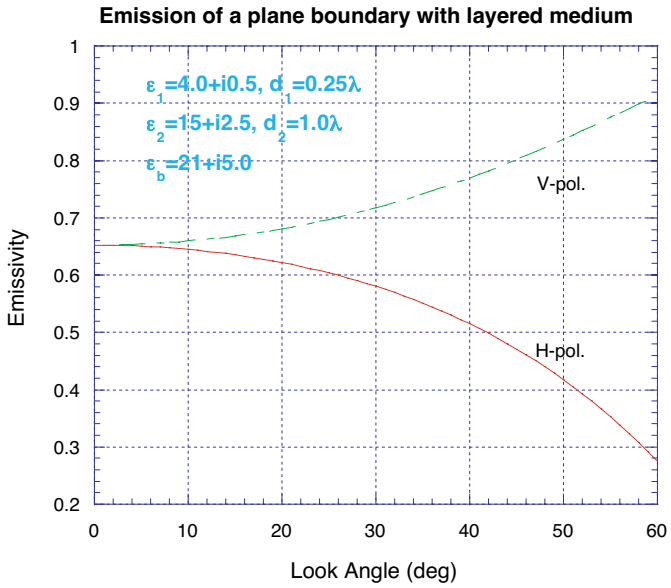

Figure 2. Emissivity of a three-layered medium ($\varepsilon_1 = 4 + i0.5$, $\varepsilon_2 = 15 + i2.5$, $d_1 = 0.25\lambda$ and $d_2 = 1.0\lambda$, $\varepsilon_b = 21 + i5$) with top plane boundary. Both H- and V-polarized cases are shown.

power for H-polarized and V-polarized cases with the look angles from 10 to 50 degrees. For comparison, results for the homogeneous surface (non-layered) are also tabulated. The table indicates that for H-polarized case, all the scattering power from the layered medium is larger than those from the non-layered surfaces for all the observed angles considered here. For V-polarized case, some angular oscillations were observed. This is possible because the reflective energy from the layered medium could be less than those from the non-layered medium [1]. Since the dielectric gradient of the three-layer medium was chosen to be intently small, it was expected that the contributions from the stratified medium were also correspondingly small. At this point, it can be argued that as the dielectric gradient becomes large, the difference of emissivities between the layered medium and non-layered medium should be large as well, as will be shown below for such cases.

To see the effects of the inhomogeneity, we increased the dielectric gradient. The rough boundary was again assumed to be Gaussian with correlation length of 1 wavelength, rms height of 0.1λ. The dielectric constants of the two layers were $\varepsilon_1 = 4+i0.5$, $\varepsilon_2 = 15+i2.5$, with each depth of $d_1 = 0.25\lambda$ and $d_2 = 1.0\lambda$ and the half-space permittivity was

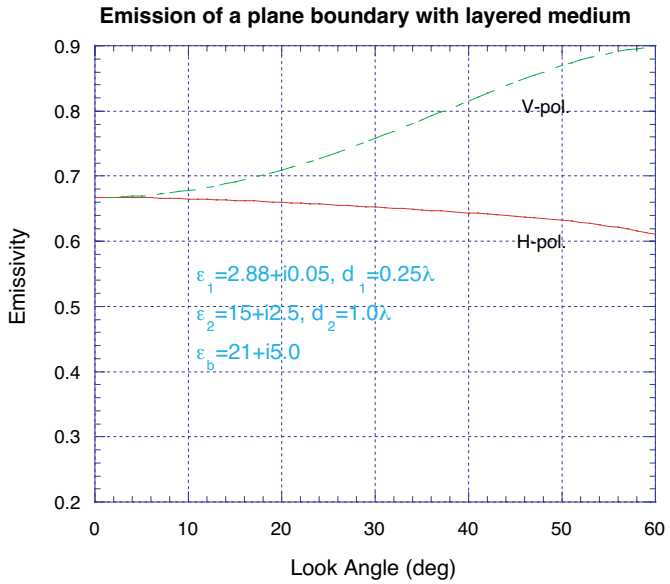

Figure 3. Emissivity of a three-layered medium ($\varepsilon_1 = 2.88 + i0.05$, $d_1 = 0.25\lambda$, $\varepsilon_2 = 15 + i2.5$, $d_2 = 1.0\lambda$, $\varepsilon_b = 21 + i5$) with top plane boundary. Both H- and V-polarized cases are shown.

Table 1. Reflectivities of non-layered (NL) and layered (L) media for H and V polarizations.

Look Angle(deg)	NL-H	L-H	NL-V	L-V
10	0.22147	0.22165	0.20768	0.20720
20	0.23395	0.23455	0.18981	0.18909
30	0.25708	0.25815	0.16304	0.16236
40	0.29520	0.29555	0.12840	0.12790
50	0.36133	0.36215	0.087704	0.087983

set to $\varepsilon_b = 21 + i5$. Fig. 4a shows the reflectivity, while Fig. 4b is the emissivity. For comparison, those of without layered medium were also plotted. At the angles smaller than around 40 degrees, the layered medium has more contributions. Overall, the layered medium has a larger reflectivity than those non-layered medium for all the look angles considered. Correspondingly, the emissivity is generally smaller for the

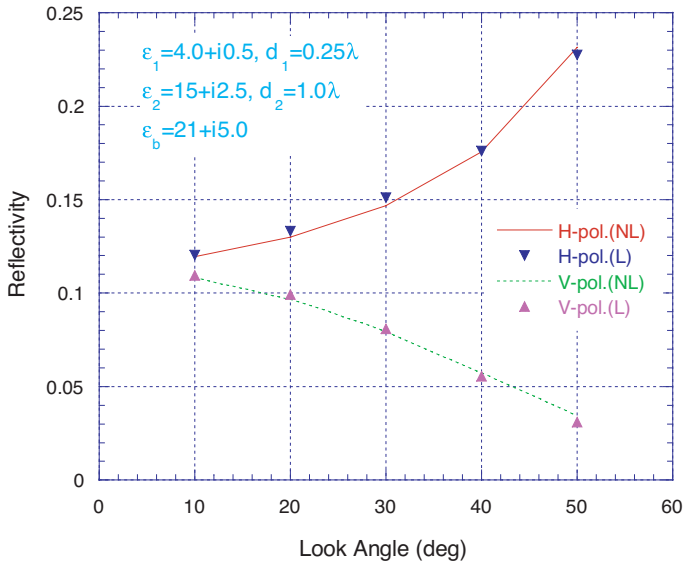

(a)

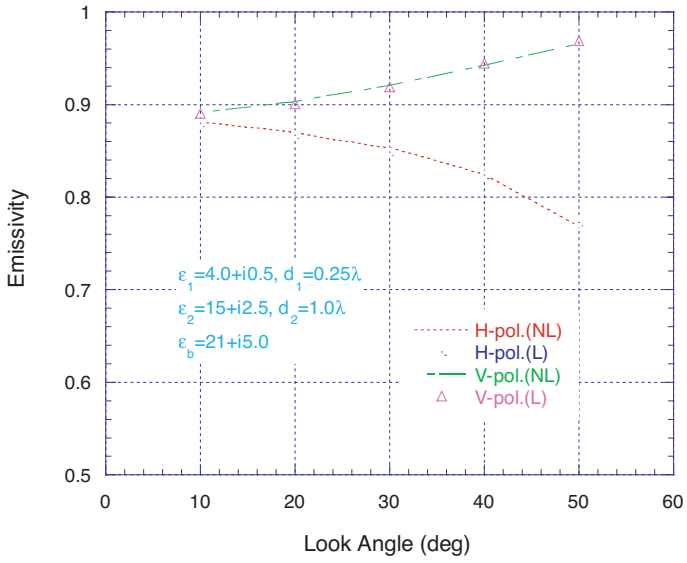

(b)

Figure 4. (a) Reflectivity and (b) emissivity of a rough surface with and without a layered medium. Three layers ($\varepsilon_1 = 4.0 + i0.5$, $d_1 = 0.25\lambda$, $\varepsilon_2 = 15 + i2.5$, $d_2 = 1.0\lambda$, $\varepsilon_b = 21 + i5$) were shown with look angle from 10 to 50 degrees.

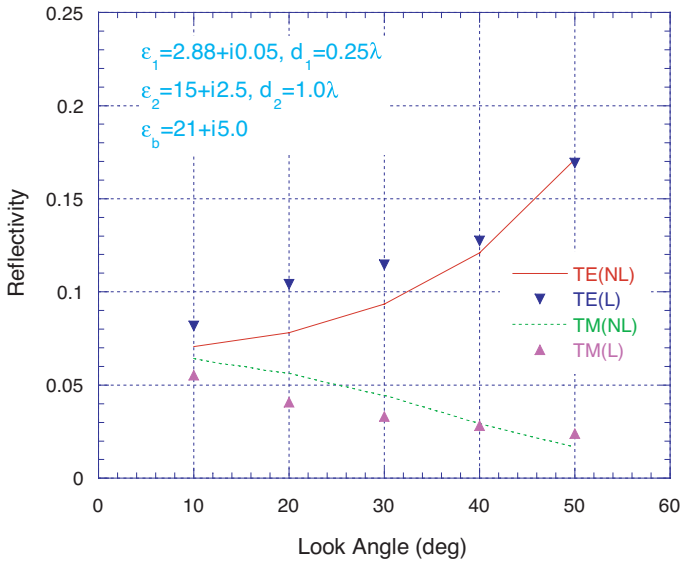

(a)

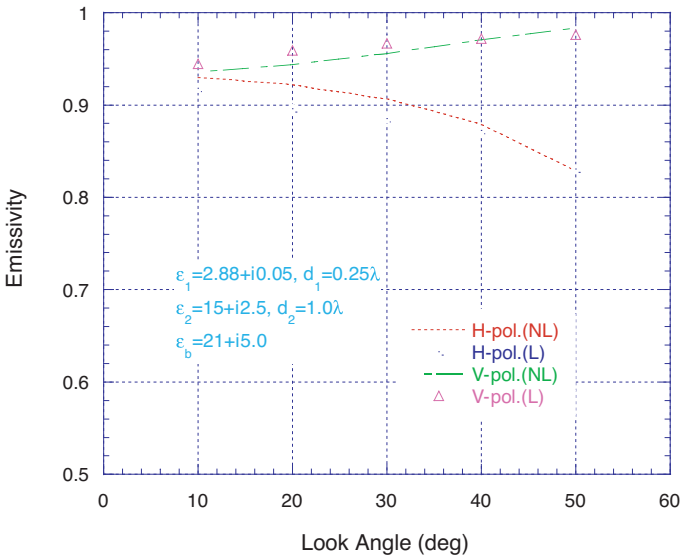

(b)

Figure 5. (a) Reflectivity and (b) emissivity of a rough surface with and without a layered medium. Three layers ($\varepsilon_1 = 2.88 + i0.05,\ d_1 = 0.25\lambda,\ \varepsilon_2 = 15 + i2.5,\ d_2 = 1.0\lambda,\ \varepsilon_b = 21 + i5$) are shown with look angle from 20 to 50 degrees.

layered medium. Compared to the case in Table 1, now, the difference between the layered and non-layered medium becomes larger with the increase of the dielectric gradients among the layers. This can be expected because in such case, the reflected part of the dyadic Green's function $\overline{\overline{G}}_1^r$ becomes more important and thus contributes more to the total part. Recall that when there is no gradient exists in the layered medium (i.e., non-layered medium), $\overline{\overline{G}}_1^r$ simply vanishes.

It must be remembered that a small change of emissivity results in large difference when converting to brightness temperature. Fig. 5 displays another set of the simulation results. The layer parameters were the same as in Fig. 4, except the dielectric constant in the first layer was $2.88 + j0.05$. The gradient between the first and the second layers was larger. Generally, the reflectivity is smaller because of smaller dielectric constant at the top layer. The difference between the layered and non-layered medium, however, is now more appreciable. The emissivity also follows the similar trends. Smaller look angle clearly generated larger difference. This was also expected since for larger look angles, the propagation paths were also longer and thus more attenuations resulted, leading to less contributions of $\overline{\overline{G}}_1^r$.

5. CONCLUSIONS

Numerical simulations of scattering of rough surfaces with an inhomogeneous layered medium by using the physics-based two-grid method combined with sparse matrix canonical grid method (PBTG-SMCG) were presented. By separating the Dyadic Green's function into a direct part and a reflected part, and reformulating the reflected part, we can apply the numerical framework of PBTG. The extension is easy and straightforward. The surface fields associated with the reflected part of the dyadic Green's function was decomposed into tangential and normal components for electric and magnetic fields. Then we can combine them with those associated with the direct part such that the structure of PBTG is applicable. Contributions from the reflected part, namely, the inhomogeneity effects of the lower medium, can be observed numerically. Explicit expressions of all the components of the reflected part were given for readily computation. Numerical scheme for implementation was also thoroughly described. In summary, a numerical simulation of the full three-dimensional rough surfaces with layered medium was proposed. The fast computation and super accuracy permits us to perform the simulations of surface reflectivity and emissivity which require strict energy conservation check. It provides an efficient tool to investigate the microwave

emission of layered medium with rough boundary such as snow and soil surfaces. The simulations show that the effect of the inhomogeneous layered medium is non-negligible and is polarization dependent.

APPENDIX A. EXPLICIT FORM OF $\vec{I}^r$ AND $\vec{F}^r$

For simple notation, let

$$\overline{\overline{G}}_1^d \equiv \begin{bmatrix} \hat{x}\hat{x}G_{xx} & \hat{x}\hat{y}G_{xy} & \hat{x}\hat{x}G_{xz} \\ \hat{y}\hat{x}G_{yx} & \hat{y}\hat{y}G_{yy} & \hat{y}\hat{z}G_{yz} \\ \hat{z}\hat{x}G_{zx} & \hat{z}\hat{y}G_{zy} & \hat{z}\hat{z}G_{zz} \end{bmatrix} \tag{A1}$$

$$\nabla \times \overline{\overline{G}}_1^d = \begin{bmatrix} \hat{x}\hat{x}D_{xx} & \hat{x}\hat{y}D_{xy} & \hat{x}\hat{x}D_{xz} \\ \hat{y}\hat{x}D_{yx} & \hat{y}\hat{y}D_{yy} & \hat{y}\hat{z}D_{yz} \\ \hat{z}\hat{x}D_{zx} & \hat{z}\hat{y}D_{zy} & \hat{z}\hat{z}D_{zz} \end{bmatrix} \tag{A2}$$

After a series of vector manipulations, we can obtain

$$\begin{aligned} I_x^r &= \hat{x} \cdot \vec{I}^r \\ &= \hat{x} \cdot (\vec{s} \times \vec{E}^i) + \hat{x} \cdot \vec{s} \times \iint \left(\nabla \times \overline{\overline{G}} \cdot \vec{I}^{r'} + i\omega\mu \overline{\overline{G}} \cdot \vec{F}^{r'} \right) dx'dy' \\ &= -E_{iy} + \iint \Big\{ \left[(-f_y D_{zx} - D_{yx}) + f'_x(-f_y D_{zz} - D_{yz}) \right] I_x^{r'} \\ &\quad + \left[(-f_y D_{zy} - D_{yy}) + f'_y(-f_y D_{zz} - D_{yz}) \right] I_y^{r'} \\ &\quad + i\omega\mu \left[(-f_y G_{zx} - G_{yx}) + f'_x(-f_y G_{zz} - G_{yz}) \right] F_x^{r'} \\ &\quad + i\omega\mu \left[(-f_y G_{zy} - G_{yy}) + f'_y(-f_y G_{zz} - G_{yz}) \right] F_y^{r'} \Big\} dx'dy' \end{aligned} \tag{A3}$$

$$\begin{aligned} I_y^r &= \hat{y} \cdot \vec{I}^r \\ &= \hat{y} \cdot (\vec{s} \times \vec{E}^i) + \hat{y} \cdot \vec{s} \times \iint \left(\nabla \times \overline{\overline{G}} \cdot \vec{I}^{r'} + i\omega\mu \overline{\overline{G}} \cdot \vec{F}^{r'} \right) dx'dy' \\ &= E_{ix} + f_x E_{iy} + \iint \Big\{ \left[(D_{xx} + f_x D_{zx}) + f'_x(D_{xz} + f_x D_{zz}) \right] I_x^{r'} \\ &\quad + \left[(D_{xy} + f_x D_{zy}) + f'_y(D_{xz} + f_x D_{zz}) \right] I_y^{r'} \\ &\quad + i\omega\mu \left[(G_{xx} + f_x G_{zx}) + f'_x(G_{xz} + f_x G_{zz}) \right] F_x^{r'} \\ &\quad + i\omega\mu \left[(G_{xy} + f_x G_{zy}) + f'_y(G_{xz} + f_x G_{zz}) \right] F_y^{r'} \Big\} dx'dy' \end{aligned} \tag{A4}$$

$$
\begin{aligned}
F_x^r &= \hat{x}\cdot\vec{F}^r \\
&= \hat{x}\cdot(\vec{s}\times\vec{H}^i)+\hat{x}\cdot\vec{s}\times\iint\left\{-i\omega\varepsilon(\overline{\overline{G}}\cdot\vec{I}^{r'})+(\nabla\times\overline{\overline{G}}\cdot\vec{F}^{r'})\right\}dx'dy' \\
&= -H_{iz}-\beta H_{iy}+\iint\Big\{-i\omega\varepsilon\left[(-f_yG_{zx}-G_{yx})+f_x'(-f_yG_{zz}-G_{yz})\right]I_x^{r'} \\
&\quad +i\omega\varepsilon\left[(-f_yG_{zy}-G_{yy})+f_y'(-f_yG_{zz}-G_{yz})\right]I_y^{r'} \\
&\quad +\left[(-f_yD_{zx}-D_{yx})+f_x'(-f_yD_{zz}-D_{yz})\right]F_x^{r'} \\
&\quad +\left[(-f_yD_{zy}-D_{yy})+f_y'(-f_yD_{zz}-D_{yz})\right]F_y^{r'}dx'dy' \qquad \text{(A5)}
\end{aligned}
$$

$$
\begin{aligned}
F_y^r &= \hat{y}\cdot\vec{F}^r \\
&= \hat{y}\cdot(\vec{s}\times\vec{H}^i)+\hat{y}\cdot\vec{s}\times\iint\left\{-i\omega\varepsilon(\overline{\overline{G}}\cdot\vec{I}^{r'})+(\nabla\times\overline{\overline{G}}\cdot\vec{F}^{r'})\right\}dx'dy' \\
&= -H_{iy}-f_yH_{iy}+\iint\{-i\omega\varepsilon\left[(G_{xx}+f_xG_{zx})+f_x'(G_{xy}+f_xG_{zy})\right]\}I_x^{r'} \\
&\quad -i\omega\varepsilon\left[(G_{xy}+f_xG_{zy})+f_y'(G_{xz}+f_xG_{zz})\right]I_y^{r'} \\
&\quad +\left[(D_{xx}+f_xD_{zx})+f_x'(D_{xy}+f_xD_{zy})\right]F_x^{r'} \\
&\quad +\left[(D_{xy}+f_xD_{zy})+f_y'(D_{xz}+f_xD_{zz})\right]F_y^{r'}dx'dy \qquad \text{(A6)}
\end{aligned}
$$

Note that

$$\hat{n}\cdot\vec{I}^r = 0 \rightarrow I_z^r = f_xI_x^r + f_yI_y^r \qquad \text{(A7)}$$

$$\hat{n}\cdot\vec{F}^r = 0 \rightarrow F_z^r = f_xF_x^r + f_yF_y^r \qquad \text{(A8)}$$

It follows that the normal components of $\vec{I}^r$ and $\vec{F}^r$ are written as, respectively

$$
\begin{aligned}
I_n^r = {} & (-f_xE_{ix}-f_yE_{iy}+E_{iz}) \\
& +\int\Big\{\left[-(f_xD_{xx}+f_yD_{yx}-D_{zx}+f_xf_x'D_{xz}+f_yf_x'D_{yz}-f_x'D_{zz}\right]I_x^{r'} \\
& +\left[f_xD_{xy}+f_yD_{yy}-D_{zy}+f_xf_x'D_{xz}+f_yf_x'D_{yz}-f_x'D_{zz}\right]I_y^{r'} \\
& -i\omega\varepsilon\left[f_xG_{xx}+f_yG_{yx}-G_{zx}+f_xf_x'G_{xz}+f_yf_x'G_{yz}-f_x'G_{zz}\right]F_x^{r'} \\
& +i\omega\varepsilon\Big[f_xG_{xy}+f_yG_{yy}-G_{zy}+f_xf_y'G_{xz}+f_yf_y'G_{yz}-f_y'G_{zz}\Big]F_y^{r'}\Big\}dx'dy' \qquad \text{(A9)}
\end{aligned}
$$

$$
\begin{aligned}
F_n^r = {} & (-f_xH_{ix}-f_yH_{iy}+H_{iz}) \\
& +\iint\Big\{(-i\omega\varepsilon)\Big[f_xG_{xx}+f_yG_{yx}-G_{zx}+f_xf_x'G_{xz}+f_yf_y'G_{yz}-f_x'G_{zz}\Big]I_x^{r'}
\end{aligned}
$$

$$+(-i\omega\varepsilon)\left[f_xG_{xy}+f_yG_{yy}-G_{zy}+f_xf'_yG_{xz}+f_yf'_yG_{yz}-f'_yG_{zz}\right]I_y^{r'}$$
$$-\left[f_xD_{xx}+f_yD_{yx}-D_{zx}+f_xf'_xD_{xz}+f_yf'_xD_{yz}-f'_xD_{zz}\right]F_x^{r'}$$
$$+\left[f_xD_{xy}+f_yD_{yy}-D_{zy}+f_xf'_yD_{xz}+f_yf'_yD_{yz}-f'_yG_{zz}\right]F_y^{r'}\Big\}dx'dy' \tag{A10}$$

APPENDIX B. EXPLICIT FORMS OF $\overline{\overline{G}}_1^r$ AND $\nabla\times\overline{\overline{G}}_1^r$

To write explicit form of (42) and (43), let $X=x-x',\ \mathcal{Y}=y-y',\ Z=z+z'+2d_1$, with $\Delta=e^{-i2k_{1z}d_1}$, and $\rho=\sqrt{X^2+\mathcal{Y}^2},\ \phi=\tan^{-1}(\mathcal{Y}/X)$. After some mathematical manipulations, we have

$$\begin{aligned}
\overline{\overline{G}}_1^r(X,\mathcal{Y},Z) = {} & \frac{i}{4\pi}\hat{x}\hat{x}\int_0^\infty dk_\rho k_\rho\frac{1}{k_{1z}}e^{ik_{1z}z} \\
& \times\left[R^{TE}\Delta\left(J'_1(k_\rho\rho)\sin^2\phi+\frac{J_1(k_\rho\rho)}{k_\rho\rho}\cos^2\phi\right)\right. \\
& \left.-R^{TM}\Delta\frac{k_{1z}^2}{k_1^2}\left(J'_1(k_\rho\rho)\cos^2\phi+\frac{J_1(k_\rho\rho)}{k_\rho\rho}\sin^2\phi\right)\right] \\
& +\frac{i}{4\pi}\hat{x}\hat{y}\int_0^\infty dk_\rho k_\rho\frac{1}{k_{1z}}e^{ik_{1z}z}\left[-R^{TE}\Delta-R^{TM}\Delta\frac{k_{1z}^2}{k_1^2}\right] \\
& \left[J'_1(k_\rho\rho)-\frac{J_1(k_\rho\rho)}{k_\rho\rho}\right]\cos\phi\sin\phi \\
& +\frac{i}{4\pi}\hat{y}\hat{x}\int_0^\infty dk_\rho k_\rho\frac{1}{k_{1z}}e^{ik_{1z}z}\left[-R^{TE}\Delta-R^{TM}\Delta\frac{k_{1z}^2}{k_1^2}\right] \\
& \left[J'_1(k_\rho\rho)-\frac{J_1(k_\rho\rho)}{k_\rho\rho}\right]\cos\phi\sin\phi+\frac{i}{4\pi}\hat{y}\hat{y}\int_0^\infty dk_\rho k_\rho\frac{1}{k_{1z}}e^{ik_{1z}z} \\
& \times\left[R^{TE}\Delta\left(J'_1(k_\rho\rho)\cos^2\phi+\frac{J_1(k_\rho\rho)}{k_\rho\rho}\sin^2\phi\right)\right. \\
& \left.-R^{TM}\Delta\frac{k_{1z}^2}{k_1^2}\left(J_1(k_\rho\rho)\cos^2\phi+\frac{J'_1(k_\rho\rho)k_{1z}^2}{k_1^2}\sin^2\phi\right)\right] \\
& -\frac{i}{4\pi}\hat{x}\hat{z}\int_0^\infty dk_\rho k_\rho\frac{1}{k_{1z}}e^{ik_{1z}z}\left[R^{TM}\Delta J_1(k_\rho\rho)\left(\frac{-k_{1z}}{k_1^2}\right)k_\rho\cos\phi\right]
\end{aligned}$$

$$
\begin{aligned}
&-\frac{i}{4\pi}\hat{z}\hat{x}\int_0^\infty dk_\rho k_\rho \frac{1}{k_{1z}} e^{ik_{1z}z}\left[R^{TM}\Delta J_1(k_\rho\rho)\left(\frac{k_{1z}}{k_1^2}\right)k_\rho\cos\phi\right]\\
&-\frac{i}{4\pi}\hat{y}\hat{z}\int_0^\infty dk_\rho k_\rho \frac{1}{k_{1z}} e^{ik_{1z}z}\left[R^{TM}\Delta J_1(k_\rho\rho)\left(\frac{-k_{1z}}{k_1^2}\right)k_\rho\sin\phi\right]\\
&-\frac{i}{4\pi}\hat{z}\hat{y}\int_0^\infty dk_\rho k_\rho \frac{1}{k_{1z}} e^{ik_{1z}z}\left[R^{TM}\Delta J_1(k_\rho\rho)\left(\frac{k_{1z}}{k_1^2}\right)k_\rho\sin\phi\right]\\
&+\frac{i}{4\pi}\hat{z}\hat{z}\int_0^\infty dk_\rho k_\rho \frac{1}{k_{1z}} e^{ik_{1z}z}\left[R^{TM}\Delta J_0(k_\rho\rho)\left(\frac{k_\rho^2}{k_1^2}\right)\right] \qquad \text{(B1)}
\end{aligned}
$$

$$
\begin{aligned}
\Delta\times\overline{\overline{G}}_1^r(X,\mathcal{Y},Z) &= \frac{i}{4\pi}\hat{x}\hat{x}\int_0^\infty dk_\rho k_\rho \frac{1}{k_{1z}} e^{ik_{1z}z}\\
&\times\left[R^{TE}\Delta\frac{k_{1z}}{k_1}\left(J_1'(k_\rho\rho)-\frac{J_1(k_\rho\rho)}{k_\rho\rho}\right)\cos\phi\sin\phi\right.\\
&\left.+\,R^{TM}\Delta\frac{k_{1z}}{k_1}\left(J_1'(k_\rho\rho)-\frac{J_1(k_\rho\rho)}{k_\rho\rho}\right)\cos\phi\sin\phi\right]\\
&+\frac{i}{4\pi}\hat{x}\hat{y}\int_0^\infty dk_\rho k_\rho \frac{1}{k_{1z}} e^{ik_{1z}z}\\
&\times\left[-R^{TE}\Delta\frac{k_{1z}}{k_1}\left(J_1'(k_\rho\rho)\cos^2\phi-\frac{J_1(k_\rho\rho)}{k_\rho\rho}\sin^2\phi\right)\right.\\
&\left.+\,R^{TM}\Delta\frac{k_{1z}}{k_1}\left(J_1(k_\rho\rho)\frac{J_1(k_\rho\rho)}{k_\rho\rho}\cos^2\phi-J_1'(k_\rho\rho)\phi\sin^2\phi\right)\right]\\
&-\frac{i}{4\pi}\hat{x}\hat{z}\int_0^\infty dk_\rho k_\rho \frac{1}{k_{1z}} e^{ik_{1z}z}\left[R^{TM}\Delta J_1(k_\rho\rho)\frac{k_\rho}{k_1}\sin\phi\right]\\
&+\frac{i}{4\pi}\hat{y}\hat{x}\int_0^\infty dk_\rho k_\rho \frac{1}{k_{1z}} e^{ik_{1z}z}\\
&\times\left[R^{TE}\Delta\left(J_1(k_\rho\rho)\frac{J_1(k_\rho\rho)}{k_\rho\rho}\cos^2\phi-J_1'(k_\rho\rho)\sin^2\phi\right)\frac{k_{1z}}{k_1}\right.
\end{aligned}
$$

$$
\begin{aligned}
&-R^{TM}\Delta\left(J_1'(k_\rho\rho)\cos^2\phi-\frac{J_1(k_\rho\rho)}{k_\rho\rho}\sin^2\phi\right)\frac{k_{1z}}{k_1}\\
&+\frac{i}{4\pi}\hat{y}\hat{y}\int_0^\infty dk_\rho k_\rho\frac{1}{k_{1z}}e^{ik_{1z}z}\left[-R^{TE}\Delta\frac{k_{1z}}{k_1}\left(J_1'(k_\rho\rho)-\frac{J_1(k_\rho\rho)}{k_\rho\rho}\right)\cos\phi\sin\phi\right.\\
&\left.-R^{TM}\Delta\frac{k_{1z}}{k_1}\left(J_1'(k_\rho\rho)-\frac{J_1(k_\rho\rho)}{k_\rho\rho}\right)\cos\phi\sin\phi\right]\\
&-\frac{i}{4\pi}\hat{y}\hat{z}\int_0^\infty dk_\rho k_\rho\frac{1}{k_{1z}}e^{ik_{1z}z}\left[-R^{TM}\Delta J_1(k_\rho\rho)\frac{k_\rho}{k_1}\cos\phi\right]\\
&-\frac{i}{4\pi}\hat{z}\hat{x}\int_0^\infty dk_\rho k_\rho\frac{1}{k_{1z}}e^{ik_{1z}z}\left[-R^{TM}\Delta J_1(k_\rho\rho)\frac{k_\rho}{k_1}\cos\phi\right]\\
&-\frac{i}{4\pi}\hat{z}\hat{y}\int_0^\infty dk_\rho k_\rho\frac{1}{k_{1z}}e^{ik_{1z}z}\left[R^{TM}\Delta J_1(k_\rho\rho)\frac{k_\rho}{k_1}\cos\phi\right] \qquad \text{(B2)}
\end{aligned}
$$

In (B1) and (B2), J_n is Bessel function of order n and J_n' is derivative of Bessel function of order n. It is noted that the $\hat{z}\hat{z}$ component is vanishing.

REFERENCES

1. Tsang, L., J. A. Kong, and R. T. Shin, *Theory of Microwave Remote Sensing*, John Wiley & Sons, 1985.
2. Chew, W. C., *Waves and Fields in Inhomogeneous Media*, IEEE Press, 1995.
3. Fung, A. K. and M. F. Chen, "Emission from an inhomogeneous layer from a rough surface," *Radio Science*, Vol. 16, 289–298, 1981.
4. Wang, J. R. and B. J. Choudhury, "Remote sensing of soil moisture content over bare fields at 1.4 GHz frequency," *J. Geophys. Res.*, Vol. 86, 5277–5282, 1981.
5. Tsang, L. and R. W. Newton, "Microwave emissions from soils with rough surfaces," *J. Geophy. Res.*, Vol. 87, No. 11, 9017–9024, Oct. 1982.
6. Wang, J. R., P. E. O'Neill, T. J. Jackson, and E. T. Engman, "Multi-frequency measurements of the effects of soil moisture, soil texture and surface roughness," *IEEE Trans. Geosci. Rem. Sens.*, Vol. GE-21, 44–51, 1983.
7. Mo, T., T. J. Schmugge, and J. R. Wang, "Calculations of the

microwave brightness temperature of rough soil surfaces: bare field," *IEEE Trans. Geosci. Remote Sensing*, Vol. GE-25, No. 1, 47–54, Jan. 1987.

8. Shi, J., J. Dozier, and H. Rott, "Snow mapping in alpine regions with synthetic aperture radar," *IEEE Transactions on Geoscience and Remote Sensing*, Vol. 32, No. 1, 152–158, 1994.
9. Shi, J., J. Wang, A. Hsu, P. O'Neill, and E. T. Engman, "Estimation of bare surface soil moisture and surface roughness parameters using L-band SAR image data," *IEEE Transactions on Geoscience and Remote Sensing*, Vol. 35, No. 5, 1254–1266, 1997.
10. Fuks, I. M. and A. G. Voronovich, "Wave diffraction by rough interfaces in an arbitrary plane layered medium," *Waves in Random Medium*, Vol. 10, 253–272, 2000.
11. Johoson, J. T., "Thermal emission from a layered medium bounded by a slightly rough interface," *IEEE Trans. Geosci. Remote Sensing*, Vol. 39, No. 2, 368–378, 2001.
12. Chen, K. S., T. D. Wu, L. Tsang, Qin Li, and J. C. Shi, "The emission of rough surfaces calculated by the Integral equation method with a comparison to a three-dimensional moment method simulations," *IEEE Trans. Geoscience and Remote Sensing*, Vol. 41, No. 1, 90–101, 2002.
13. Pelosi, G. and R. Coccioli, "A finite element approach for scattering from inhomogeneous media with a rough interface," *Waves in Random Media*, Vol. 7, 119–127, 1997.
14. Giovannini, H., M. Saillard, and A. Sentenac, "Numerical study of scattering from rough inhomogeneous films," *J. Opt. Soc. Am, A*, Vol. 15, No. 5, 1182–1191, 1998.
15. Tsang, L., C. H. Chan, and K. Pak, "Backscattering enhancement of a two-dimensional random rough surface (three-dimensional scattering) based on Monte Carlo simulations," *J. of Optical Society of America A*, Vol. 11, No. 2, 711–715, 1994.
16. Johnson, J., L. Tsang, R. Shin, K. Pak, C. H. Chan, A. Ishimaru, and Y. Kuga, "Backscattering enhancement of electromagnetic waves from two-dimensional perfectly conducting random rough surfaces: A Comparison of Monte Carlo simulations with experimental data," *IEEE Trans. Antennas Propagat.*, Vol. 44, 748–756, 1996.
17. Tsang, L. and Q. Li, "Numerical solution of scattering of waves by lossy dielectric surfaces using a physics-based two-grid method," *Microwave Opt. Technol. Lett.*, Vol. 16, No. 6, 356–364, December 20, 1997.

18. Li, Q., C. H. Chan, and L. Tsang, "Monte-Carlo simulations of wave scattering from lossy dielectric random rough surfaces using the physics-based two-gird method and canonical grid method," *IEEE Trans. Antennas Propagat.*, Vol. 47, No. 4, 752–763, April 1999.
19. Tsang, L., J.-H. Cha, and J. R. Thomas, "Electric fields of spatial Green's functions of microstrip structures and applications to the calculations of impedance matrix elements," *Microwave and Optical Technology Letters*, Vol. 20, No. 2, 90–97, 1999.
20. Tsang, L., J. A. Kong, K. H. Ding, and C. O. Ao, *Scattering of Electromagnetic Waves*, Volume II: Numerical Simulations, John Wiley & Sons, 2001.